\




## Topology of a parity-time symmetric non-Hermitian rhombic lattice

Shumai Zhang(张舒迈), Liang Jin(金亮), and Zhi Song(宋智)
**Citation:**Chin. Phys. B, 2022, 31 (**1**): 010312. DOI: 10.1088/1674-1056/ac364a
Journal homepage: http://cpb.iphy.ac.cn; http://iopscience.iop.org/cpb

**What follows is a list of articles you may be interested in**

---

## Topological properties of non-Hermitian Creutz ladders

Hui-Qiang Liang(梁辉强) and Linhu Li(李林虎)
Chin. Phys. B, 2022, 31 (**1**): 010310. DOI: 10.1088/1674-1056/ac3991

## Non-Hermitian Weyl semimetals: Non-Hermitian skin effect and non-Bloch bulk-boundary correspondence

Xiaosen Yang(杨孝森), Yang Cao(曹阳), and Yunjia Zhai(翟云佳)
Chin. Phys. B, 2022, 31 (**1**): 010308. DOI: 10.1088/1674-1056/ac3738

## Photoinduced Weyl semimetal phase and anomalous Hall effect in a three-dimensional topological insulator

Meng-Nan Chen(陈梦南) and Wen-Chao Chen(陈文潮)
Chin. Phys. B, 2021, 30 (**11**): 110308. DOI: 10.1088/1674-1056/abff29

## Non-Hermitian quasicrystal in dimerized lattices

Longwen Zhou(周龙文) and Wenqian Han(韩雯岍)
Chin. Phys. B, 2021, 30 (**10**): 100308. DOI: 10.1088/1674-1056/ac1efc

## Review of quantum simulation based on Rydberg many-body system

Zheng-Yuan Zhang(张正源), Dong-Sheng Ding(丁冬生), and Bao-Sen Shi(史保森)
Chin. Phys. B, 2021, 30 (**2**): 020307. DOI: 10.1088/1674-1056/abd744

---

**SPECIAL TOPIC — Non-Hermitian physics**

# Topology of a parity–time symmetric non-Hermitian rhombic lattice

Shumai Zhang(张舒迈), Liang Jin(金亮)[†], and Zhi Song(宋智)

*School of Physics, Nankai University, Tianjin* 300071, *China*

(Received 19 August 2021; revised manuscript received 17 October 2021; accepted manuscript online 4 November 2021)

We investigate the topological properties of a trimerized parity–time ($\mathcal{PT}$) symmetric non-Hermitian rhombic lattice. Although the system is $\mathcal{PT}$-symmetric, the topology is not inherited from the Hermitian lattice; in contrast, the topology can be altered by the non-Hermiticity and depends on the couplings between the sublattices. The bulk–boundary correspondence is valid and the Bloch bulk captures the band topology. Topological edge states present in the two band gaps and are predicted from the global Zak phase obtained through the Wilson loop approach. In addition, the anomalous edge states compactly localize within two diamond plaquettes at the boundaries when all bands are flat at the exceptional point of the lattice. Our findings reveal the topological properties of the $\mathcal{PT}$-symmetric non-Hermitian rhombic lattice and shed light on the investigation of multi-band non-Hermitian topological phases.

**Keywords:** topological phase, $\mathcal{PT}$ symmetry, Wilson loop

**PACS:** 03.65.Vf, 03.65.–w **DOI:** 10.1088/1674-1056/ac364a

## 1. Introduction

In recent years, parity–time ($\mathcal{PT}$) symmetry has attracted increasing attention in non-Hermitian quantum mechanics.[1–11] $\mathcal{PT}$-symmetric non-Hermitian systems, which may possess entirely real spectra,[12] have been widely explored in the optical waveguides, resonators, and cold atoms in optical lattices. The exceptional point (EP), known as the $\mathcal{PT}$-symmetric phase transition point, indicates the transition between the exact $\mathcal{PT}$-symmetric phase and the broken $\mathcal{PT}$-symmetric phase.[13–15] The EP means not only a bifurcation point of the energy bands, but also the eigenstate coalescence at the defective Hamiltonian.[16–22] The EP has potential application in the sensing.[23]

The investigation of topology has been extended to non-Hermitian physics.[24–47] Topological systems are of great significance in the condensed-matter physics.[48–66] The researches on non-Hermitian Su–Schrieffer–Heeger (SSH) chain, Chern insulator, and nodal-line semimetals have received great interests.[67–75] As the progress on optical realization of the topological systems, the field of topological photonics has been stimulated.[76] Edge states,[77,78] band theory,[79,80] and topological invariants[81–87] are major focuses in topological physics. The topological invariant, obtained from the Bloch bulk, characterizes the feature of energy bands.[83] The existence of edge states under the open boundary condition (OBC) is predictable by topological invariants under the periodic boundary condition (PBC), which is referred to as the bulk–boundary correspondence. The bulk–boundary correspondence is invalid in the non-Hermitian systems[88] when the non-Hermitian Aharonov–Bohm effect present,[89] and different approaches to find the topological invariant are developed.[89–91]

In this paper, we investigate the topological properties of a $\mathcal{PT}$-symmetric non-Hermitian rhombic lattice. The non-Hermitian rhombic lattice is trimerized and has a quarter of a magnetic flux quantum enclosed in each triangular plaquette, where the balanced gain and loss present. Although the lattice has $\mathcal{PT}$ symmetry, the topological features are not inherited from the Hermitian rhombic lattice and the non-Hermiticity alters the band topology. The bulk–boundary correspondence of the non-Hermitian rhombic lattice is valid and the Bloch bulk captures the band topology. The topology is characterized by the global Zak phase, which predicts the presence of the topological edge states decaying from the lattice boundaries. The rhombic lattice supports a spectrum fully consisting of dispersiveless flat bands at the proper condition. Consequently, we find the anomalous edge states that compactly localize in two diamond plaquettes at the boundaries under the destructive interference.

The remainder of the paper is organized as follows. In Section 2, the $\mathcal{PT}$-symmetric non-Hermitian rhombic lattice model and the energy bands are presented. In Section 3, the topological edge states and anomalous edge states in the non-Hermitian rhombic lattice are investigated. In Section 4, the global Zak phase is introduced and predicts the nontrivial band topology. In Section 5, the conclusion is summarized and the prospect is discussed.

[†]Corresponding author. E-mail: jinliang@nankai.edu.cn

© 2022 Chinese Physical Society and IOP Publishing Ltd 

## 2. Energy bands of the non-Hermitian rhombic lattice

**Rhombic lattice** The non-Hermitian rhombic lattice is depicted in Fig. 1(a), it is translationally invariant in the horizontal direction and is a trimerized lattice with three sublattices $\{A,B,C\}$. Sublattice $A$ is passive, and sublattices $B$ and $C$ have gain and loss with rates $\gamma$. The gain and loss are staggered in the translational invariant direction. Sublattice $A$ couples to sublattices $B$ and $C$ at the coupling strengths $g_1$ and $g_2$, and the Peierls phase factor $e^{i\Phi}$ presents in the coupling with arrow, resulting in the synthetic magnetic flux $2\Phi$ enclosed in the diamond plaquette, where $\Phi=\pi/2$. The coupling between the sublattices $B$ and $C$ is $\delta$. The parameters are chosen $g_1, g_2, \gamma$ and $\delta>0$ without loss of generality. The unit cell of the non-Hermitian rhombic lattice is the two nearby triangular plaquettes containing six sites.

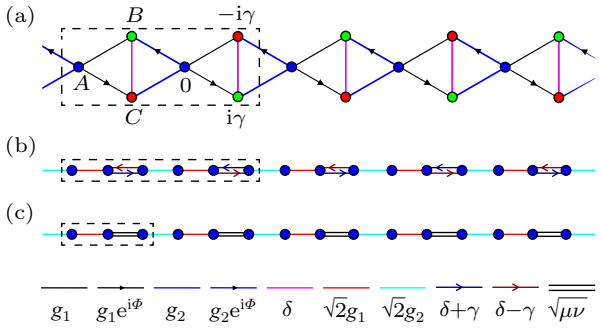



**Fig. 1.** (a) Schematic of the non-Hermitian rhombic lattice. The solid black (blue) lines represent reciprocal couplings $g_1$ ($g_2$). The black (blue) lines with arrows indicate nonreciprocal couplings, being $g_1e^{i\Phi}$ ($g_2e^{i\Phi}$) for photons tunneling along the arrow and $g_1e^{-i\Phi}$ ($g_2e^{-i\Phi}$) for photons tunneling against the arrow with $\Phi=\pi/2$. The vertical coupling $\delta$ between sublattices $B$ and $C$ is in magenta. The sites in blue are passive and sites in green (red) have gain (loss). (b) Schematic of the non-Hermitian chain with nonreciprocal couplings $\delta\pm\gamma$. (c) Schematic of the equivalent trimerized chain with reciprocal coupling $\sqrt{\mu\nu}$. The unit cell is enclosed by the black solid box.

**Bulk Bloch Hamiltonian** We consider an equivalent Bloch Hamiltonian with simple structure to investigate the topological features of the non-Hermitian rhombic lattice, because of the complexity caused by multiple components working in the rhombic chain. The foundation of the equivalent lattice is the Bloch Hamiltonian $H_k$ of the non-Hermitian rhombic lattice obtained by applying Fourier transformation to the real-space Hamiltonian,

$$H_k=\begin{pmatrix} 0 & g_1 & G_1^* & 0 & G_2^*e^{-ik} & g_2e^{-ik} \\ g_1 & i\gamma & \delta & G_2 & 0 & 0 \\ G_1 & \delta & -i\gamma & g_2 & 0 & 0 \\ 0 & G_2^* & g_2 & 0 & g_1 & G_1^* \\ G_2e^{ik} & 0 & 0 & g_1 & -i\gamma & \delta \\ g_2e^{ik} & 0 & 0 & G_1 & \delta & i\gamma \end{pmatrix}, \tag{1}$$

where $G_1=g_1e^{i\Phi}$ and $G_2=g_2e^{i\Phi}$.

Technologically, there are two consecutive steps to acquire the equivalent lattice. The first step is to obtain the 1D chain $H_k'$ with asymmetric couplings depicted in Fig. 1(b). Under a unitary transformation $H_k'=U_1^{-1}H_kU_1$ with

$$U_1=\frac{1}{\sqrt{2}}\begin{pmatrix} \sqrt{2} & 0 & 0 & 0 & 0 & 0 \\ 0 & 1 & i & 0 & 0 & 0 \\ 0 & i & 1 & 0 & 0 & 0 \\ 0 & 0 & 0 & \sqrt{2} & 0 & 0 \\ 0 & 0 & 0 & 0 & 1 & i \\ 0 & 0 & 0 & 0 & i & 1 \end{pmatrix}, \tag{2}$$

the Bloch Hamiltonian $H_k$ changes into

$$H_k'=\begin{pmatrix} 0 & \sqrt{2}g_1 & 0 & 0 & 0 & \sqrt{2}g_2e^{-ik} \\ \sqrt{2}g_1 & 0 & \delta-\gamma & 0 & 0 & 0 \\ 0 & \delta+\gamma & 0 & \sqrt{2}g_2 & 0 & 0 \\ 0 & 0 & \sqrt{2}g_2 & 0 & \sqrt{2}g_1 & 0 \\ 0 & 0 & 0 & \sqrt{2}g_1 & 0 & \delta+\gamma \\ \sqrt{2}g_2e^{ik} & 0 & 0 & 0 & \delta-\gamma & 0 \end{pmatrix}. \tag{3}$$

$U_1$ is a block diagonal matrix composed of $3\times3$ matrix $I_1\oplus\left[(\sigma_0+i\sigma_x)/\sqrt{2}\right]$ with identity matrices $I_1$, $\sigma_0$ and the Pauli matrix $\sigma_x$. $\sqrt{\mu/\nu}=e^{\phi}$ and $\sqrt{\nu/\mu}=e^{-\phi}$ indicate an imaginary gauge field effectively applied to the reciprocal coupling $\sqrt{\mu\nu}$ for the couplings $\mu=\delta-\gamma$ and $\nu=\delta+\gamma$, respectively. However, the imaginary magnetic flux does not accumulate along the translational invariant direction with the presence of alternately introduced asymmetric couplings $\delta\pm\gamma$, which induces that the accumulated factor $e^{\pm\phi}$ cancel each other in every unit cell.[89] That is, the net imaginary magnetic flux is zero under PBC. The imaginary magnetic flux also vanishes without the enclosed imaginary magnetic field under OBC. Thus, the imaginary gauge field does not affect the energy band of the rhombic lattice under either the periodic boundary condition or the open boundary condition.

The second step removes the imaginary gauge field $\phi$ (the phase factor $e^{\pm\phi}$ in the asymmetric couplings $\delta\pm\gamma$) in $H_k'$. Under a similarity transformation $H_k''=U_2^{-1}H_k'U_2$ with

$$U_2=\begin{pmatrix} 1/\sqrt{\nu} & 0 & 0 & 0 & 0 & 0 \\ 0 & 1/\sqrt{\nu} & 0 & 0 & 0 & 0 \\ 0 & 0 & 1/\sqrt{\mu} & 0 & 0 & 0 \\ 0 & 0 & 0 & 1/\sqrt{\mu} & 0 & 0 \\ 0 & 0 & 0 & 0 & 1/\sqrt{\mu} & 0 \\ 0 & 0 & 0 & 0 & 0 & 1/\sqrt{\nu} \end{pmatrix}, \tag{4}$$

the Bloch Hamiltonian $H_k'$ changes into

$$H_k''=\begin{pmatrix} 0 & \sqrt{2}g_1 & 0 & 0 & 0 & \sqrt{2}g_2e^{-ik} \\ \sqrt{2}g_1 & 0 & \sqrt{\mu\nu} & 0 & 0 & 0 \\ 0 & \sqrt{\mu\nu} & 0 & \sqrt{2}g_2 & 0 & 0 \\ 0 & 0 & \sqrt{2}g_2 & 0 & \sqrt{2}g_1 & 0 \\ 0 & 0 & 0 & \sqrt{2}g_1 & 0 & \sqrt{\mu\nu} \\ \sqrt{2}g_2e^{ik} & 0 & 0 & 0 & \sqrt{\mu\nu} & 0 \end{pmatrix}. \tag{5}$$

The lattice with reciprocal couplings is schematically depicted in Fig. 1(c) in real space, where the repeat unit contains three

sites. Therefore, the Bloch Hamiltonian of the equivalent chain depicted in Fig. 1(c) is reduced to

$$h_k = \begin{pmatrix} 0 & \sqrt{2}g_1 & \sqrt{2}g_2 e^{-ik} \\ \sqrt{2}g_1 & 0 & \sqrt{\mu\nu} \\ \sqrt{2}g_2 e^{ik} & \sqrt{\mu\nu} & 0 \end{pmatrix}, \tag{6}$$

in the momentum space. At $\mu\nu > 0$, that is, when the gain/loss rate is weak $\gamma < \delta$, the equivalent lattice is Hermitian with a fully real spectrum, reduces into a generalized SSH model with a uniform trimer cell at $g_1 = g_2 = g$ and supports topological edge modes with energy $\pm\sqrt{2}g$ in the nontrivial region.[92] At $\mu\nu < 0$, that is, when the gain/loss rate is strong $\gamma > \delta$, the coupling $\sqrt{\mu\nu}$ reduces to an anti-$\mathcal{PT}$-symmetric reciprocal imaginary coupling,[93] the lattice becomes non-Hermitian and the energy spectrum is fully complex.

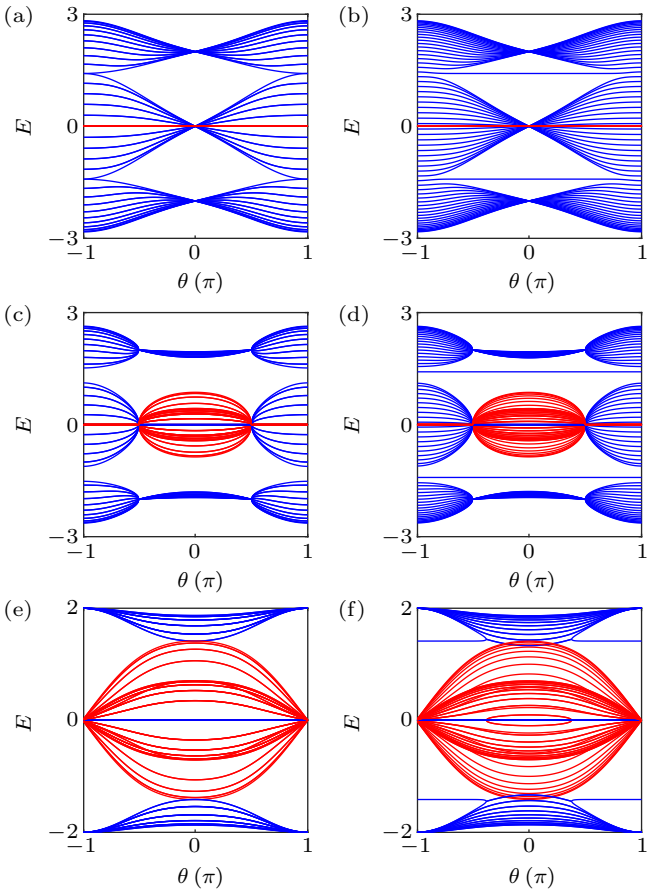



**Fig. 2.** Energy bands of the real-space rhombic lattice at different non-Hermiticity $\gamma$ under PBC (left panels) and OBC (right panels). The real (imaginary) part of the band energy is in blue (red). The lattice model has 10 unit cells, being 60 sites in total. The parameters are $g_1 = g_2 = 1$, $\delta = 1 - (1/2)\cos\theta$ with (a), (b) $\gamma = 1/2$; (c), (d) $\gamma = 1$; (e), (f) $\gamma = 3/2$.

**Energy bands** The non-Hermitian rhombic lattice has a special parameter point $\delta = \gamma$ that all the energy bands are flat. It is worth noting that the point is the exceptional point of the non-Hermitian rhombic lattice, where all the energy levels coalesce at energies 0 and $\pm\sqrt{2g_1^2 + 2g_2^2}$. The exceptional points occur at $\theta = 0$ for Fig. 2(a), $\theta = \pm\pi/2$ for Fig. 2(c), and $\theta = \pm\pi$ for Fig. 2(e) under PBC. Moreover, $\gamma < \delta$ and $\gamma > \delta$ correspond to the exact $\mathcal{PT}$-symmetric phase and the broken $\mathcal{PT}$-symmetric phase, respectively. The bulk–boundary correspondence for the non-Hermitian rhombic lattice is valid and predicts the existence of edge states in the band gaps under OBC. Distinct from the energy spectra in the left panel, the isolated bands with energy $\pm\sqrt{2}g_1$ in Figs. 2(b), 2(d), and 2(f) are known as the edge states, resulted from the open boundary condition. The non-Hermiticity persists in the quasi-1D rhombic lattice when $\gamma \neq 0$. The trimerized chain in Fig. 1(c) is Hermitian when $\gamma < \delta$ because the reciprocal coupling $\sqrt{\mu\nu}$ is real and is non-Hermitian when $\gamma > \delta$ because the reciprocal coupling $\sqrt{\mu\nu}$ is imaginary. However, the energy spectrum of the lattice in Fig. 1(a) is in accordance with that in Fig. 1(c) due to the equivalence of the two models.

## 3. Edge states

**Topological edge states** In this section, we study the edge states of the non-Hermitian rhombic lattice. In general case, we retrieve the topological properties of the non-Hermitian rhombic lattice through studying the equivalent chain in Eq. (6). The band energies are determined from the cubic equation $E_k^3 - \left(2g_1^2 + 2g_2^2 + \mu\nu\right)E_k - 4g_1g_2\sqrt{\mu\nu}\cos k = 0$ for the equivalent lattice. The existence of edge states depends on the coupling strength truncated at the open boundary. If $\sqrt{2}g_2$ is larger than either of the other two coupling strengths $\sqrt{2}g_1$ or $|\sqrt{\mu\nu}|$, the edge state appears: for $g_1 < g_2$, two edge states with energy $\pm\sqrt{\mu\nu}$ exist and localize at the right boundary; for $\left|\delta^2 - \gamma^2\right| < 2g_2^2$, two edge states with energy $\pm\sqrt{2}g_1$ exist and localize at the left boundary.

Furthermore, different situations of the band spectrum with left and right edge states are presented in Fig. 3, which verifies the conclusion about the edge states. In Fig. 3(a), the energy bands with different types of edge states under OBC are shown. In Fig. 3(b), $\sqrt{\delta^2 - \gamma^2} < \sqrt{2}g_2 < \sqrt{2}g_1$, a pair of edge states with energy $\pm\sqrt{2}g_1$ locate at the left boundary. In Fig. 3(c), $\sqrt{2}g_1 < \sqrt{2}g_2 < \sqrt{\delta^2 - \gamma^2}$, a pair of edge states with energy $\pm\sqrt{\delta^2 - \gamma^2}$ locate at the right boundary. In Fig. 3(d), $\sqrt{2}g_2$ is the largest, and two pairs of edge states exist. The amplitudes of the edge states evanescently decay as the index of the unit cell. The specific conditions for different types of edge states are described in Fig. 4, where the presence of a pair of edge states, two pairs of edge states, and the absence of edge state are shown. In Fig. 4, results of the existence of edge states altered by reciprocal coupling $\delta$ and non-Hermiticity $\gamma$ are the same. In the Hermitian case $\gamma = 0$, the appearance of edge states is constrained by two conditions: for $g_1 < g_2$, two edge states with energy $\pm\delta$ localize at the right boundary; for $\delta < \sqrt{2}g_2$, two edge states with energy $\pm\sqrt{2}g_1$ localize at the left boundary.

**Anomalous edge states** The energy bands at the EP are dispersiveless and all the eigenstates are compactly localized.

This is a consequence of the destructive interference at the appropriate match of couplings, gain and loss, and the synthetic magnetic flux enclosed in the plaquette. The corresponding edge state still appears at the EP of the rhombic lattice, but the edge state is anomalous, only localized in two diamond plaquettes at the boundary.

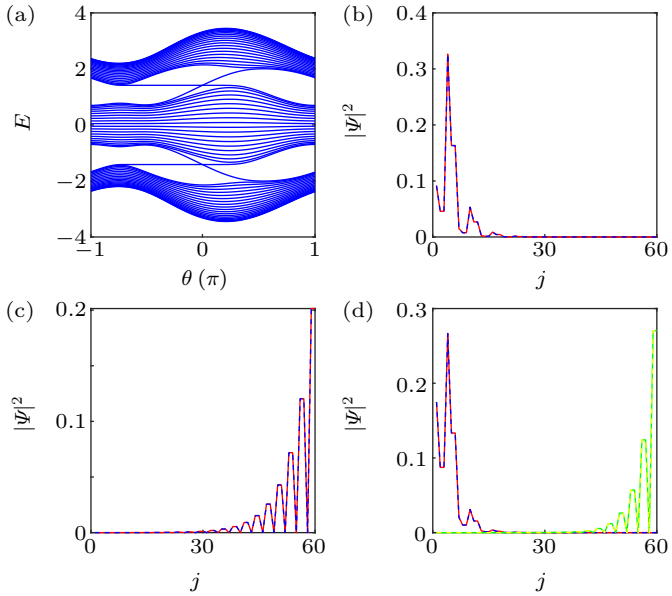



**Fig. 3.** Energy bands and edge-state amplitudes of the non-Hermitian rhombic lattice under OBC. (a) Energy bands at parameters $g_1 = \gamma = 1$, $\delta = \sqrt{3} + (1/2)\sin\theta$ and $g_2 = 1 + (1/2)\cos\theta$. All bands are entirely real with $\theta$ ranging from $-\pi$ to $\pi$. The non-Hermitian model includes 10 unit cells with 60 sites. The horizontal axis indicates the site number. The amplitudes of edge states localized at the boundaries are numerically depicted at (b) $\theta = -0.6\pi$, (c) $\theta = 0.3\pi$, and (d) $\theta = -0.1\pi$.

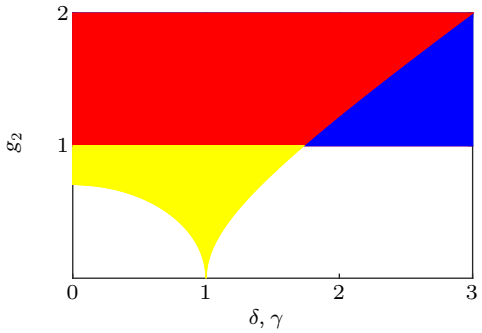



**Fig. 4.** Phase diagram of the non-Hermitian rhombic lattice in the $g_2$–$\delta$ ($g_2$–$\gamma$) plane. The parameters are $g_1 = \gamma = 1$ ($g_1 = \delta = 1$). Phase diagram in the $g_2$–$\delta$ plane is the same as that in the $g_2$–$\gamma$ plane. The yellow (blue) region has a pair of left (right) edge states with energy $\pm\sqrt{2}g_1$ ($\pm\sqrt{\delta^2-\gamma^2}$). The red area has two pairs of edge states with energies $\pm\sqrt{2}g_1$ and $\pm\sqrt{\delta^2-\gamma^2}$. The white region has no edge states.

The non-Hermitian rhombic lattice reduces to the standard Hermitian rhombic lattice at $\delta = \gamma = 0$, the eigenvalues of the Hermitian rhombic lattice are independent of the momentum $k$, the spectrum of the Hermitian rhombic lattice is constituted by three flat bands $\left\{0, \pm\sqrt{2g_1^2 + 2g_2^2}\right\}$, and the eigenstates are compactly localized in two diamond plaquettes, being $\{0, -g_1, \mathrm{i}g_1; 0, -\mathrm{i}g_2, g_2\}$ for the flat-band energy 0 and $\left\{0, g_2, -\mathrm{i}g_2; \mp\mathrm{i}\sqrt{2g_1^2 + 2g_2^2}, -\mathrm{i}g_1, g_1\right\}$ for the flat-band energy $\pm\sqrt{2g_1^2 + 2g_2^2}$. The flat bands and the localization of their eigenstates are consequence of the destructive interference induced by the $\pi$ magnetic flux enclosed in each diamond plaquette.

It is worth pointing out that the eigenstates are still localized within two boundary plaquettes under the open boundary condition, which indicates that the edge states are localized, refereed to as the anomalous edge states. Notably, these features are unchanged in the $\mathcal{PT}$-symmetric non-Hermitian generalization at $\delta = \gamma$. The formation mechanism of the anomalous edge states is the destructive interference, and the formation mechanism is greatly different from the formation mechanism of the topological edge states, which is induced by the difference in the lattice coupling strengths. Notably, both the topological edge states and the anomalous edge states exist at the EP of the rhombic lattice. The zero-energy anomalous edge state localized at the left boundary of the non-Hermitian rhombic lattice is schematically illustrated in Fig. 5(a), and the anomalous edge state with nonzero energy $\pm\sqrt{2g_1^2 + 2g_2^2}$ localized at the right boundary is illustrated in Fig. 5(b). In the following, we study the topological characterization to further unveil the topological properties of the $\mathcal{PT}$-symmetric non-Hermitian rhombic lattice.

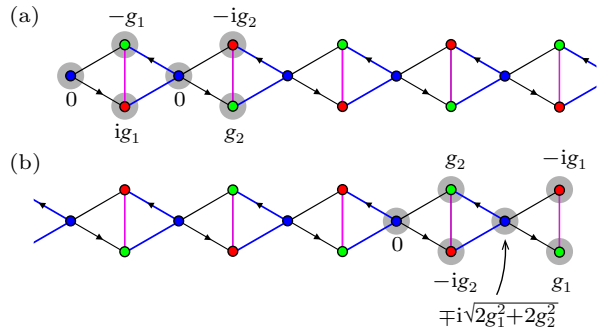



**Fig. 5.** (a) The anomalous edge state with energy 0 localized at the left boundary of the non-Hermitian rhombic lattice. (b) The anomalous edge state with energy $\pm\sqrt{2g_1^2 + 2g_2^2}$ localized at the right boundary of the non-Hermitian rhombic lattice.

## 4. Topological characterization

The geometric phase reflects the topological property of the non-Hermitian rhombic lattice from another aspect in contrast to the edge states. The Zak phase for the non-Hermitian system is analytically generalized along the closed loop $L$,

$$\Gamma_n = \mathrm{i}\oint_{2L} \langle \tilde{u}_n(k)| \frac{\partial}{\partial k} |u_n(k)\rangle \, \mathrm{d}k, \tag{7}$$

with $k$ constrained in the momentum space and the integer $n \in [1,6]$ indicating the index of all the six energy bands. $|u_n(k)\rangle$ and $|\tilde{u}_n(k)\rangle$ are eigenstates of Hamiltonians $H_k$ and $H_k^\dagger$, satisfying $H_k|u_n(k)\rangle = E_k|u_n(k)\rangle$ and $H_k^\dagger|\tilde{u}_n(k)\rangle = E_k^*|\tilde{u}_n(k)\rangle$, respectively. $|u_n(k)\rangle$ and $|\tilde{u}_n(k)\rangle$ constitute a set of biorthogonal basis obeying $\langle\tilde{u}_m(k)|u_n(k)\rangle = \delta_{mn}$. The momentum vector traces out the closed loop $L$ in the momentum space.[94,95]

The integration path $2L$ indicates two times of circling in the parameter space, to ensure the wavefunctions of energy bands come back to their initial conditions.[20] The energy levels have pairwise interchange after one circle and are restored after two circles, which is numerically demonstrated in the left panel of Fig. 6. In the following, we introduce the numerical implementation of the Zak phase in the bulk. We divide the two loops into $N$ small segments and consider a $6\times 6$ matrix $A_{k_i}$ for a segment from $k_i$ to $k_{i+1}$,

$$A_{k_i}=\begin{pmatrix} \langle\tilde{u}_1(k_i)|u_1(k_{i+1})\rangle & \cdots & \langle\tilde{u}_1(k_i)|u_6(k_{i+1})\rangle \\ \vdots & \ddots & \vdots \\ \langle\tilde{u}_6(k_i)|u_1(k_{i+1})\rangle & \cdots & \langle\tilde{u}_6(k_i)|u_6(k_{i+1})\rangle \end{pmatrix}, \quad (8)$$

where the integer $i\in[1,N]$ and $k_{N+1}=k_1$. The matrix $A$ is defined as the product of matrices $A_{k_i}$ for all small segments with the employment of the Wilson loop approach,[96]

$$A=\prod_{i=1}^{N}A_{k_i}. \quad (9)$$

The eigenvalues of the $6\times 6$ matrix $A$ are denoted as $a_n$, where the subscripts $n=1$, 2, 3, 4, 5 and 6 represent different energy bands.

For each energy band, the accumulated Zak phase obtained via the Wilson loop approach is

$$\Gamma_n'=-\arg a_n. \quad (10)$$

The Zak phase associated with each energy band of the non-Hermitian rhombic lattice is not an integer over $\pi$ in general case; however, the summation of the Zak phase for all the bands, which is referred to as the global Zak phase, is an integer over $\pi$ and considered as a topological invariant. We give the expression of global Zak phase for the system

$$\Gamma'=\sum_{n=1}^{6}\Gamma_n'. \quad (11)$$

The Zak phase for each energy band is traditionally introduced as

$$\Gamma_n=-\arg\prod_{i=1}^{N}\langle\tilde{u}_n(k_i)|u_n(k_{i+1})\rangle. \quad (12)$$

The corresponding expression of global Zak phase for the system is

$$\Gamma=\sum_{n=1}^{6}\Gamma_n. \quad (13)$$

Notably, $\Gamma_n\neq\Gamma_n'$ from their definitions; however, the summation of all eigenvalues of a matrix equals to the trace of the matrix, that is, the global Zak phase $\Gamma=\Gamma'$ can also be obtained via the Wilson loop approach.

The global Zak phase of the non-Hermitian rhombic lattice in both topological trivial and topological nontrivial phases are exemplified by the solid black lines in the right panel of Fig. 6, which presents the whole process of global Zak phase accumulation along the path integral in the parameter space. Topological edge states present in the region with nonzero global Zak phase $8\pi$, and the $8\pi$ Zak phase indicates topological edge states presenting in both two band gaps. In contrast, topological edge states are absent and the global Zak phase is 0. The numerical simulation of the Wilson loop approach is depicted by the red dashed lines in the right panel of Fig. 6, which are exactly in accord with the solid black lines. By employing the Wilson loop approach, the global Zak phase accumulated along two closed circles is $8\pi$ in the nontrivial phase, while the global Zak phase accumulated along two closed circles is 0 in the trivial phase.

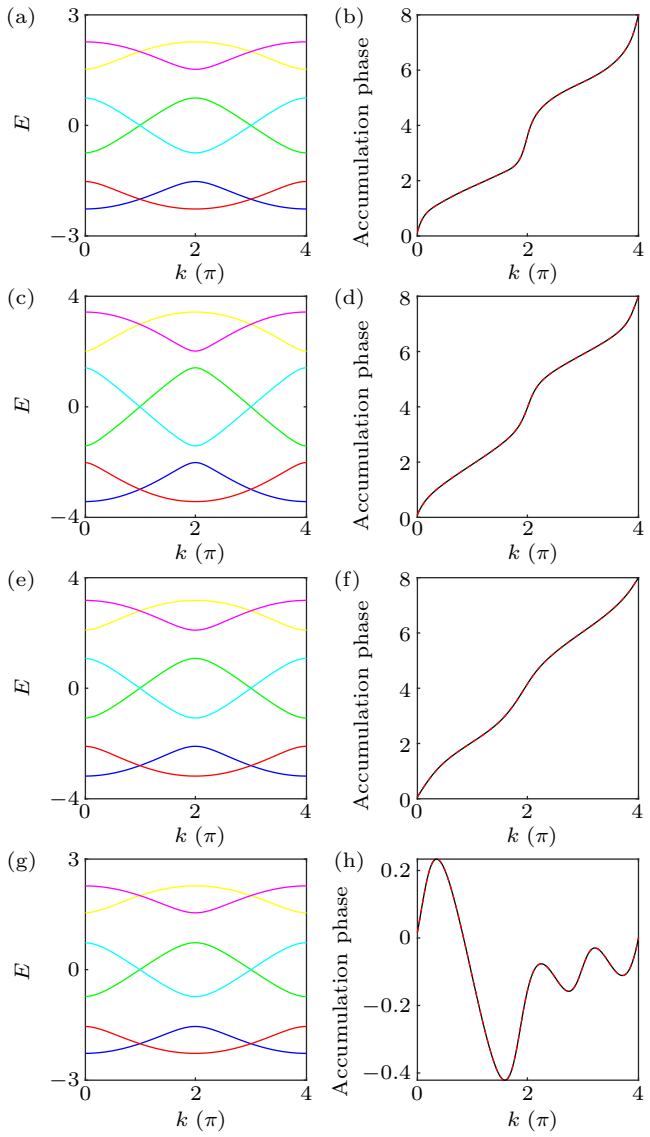



**Fig. 6.** Energy bands in momentum space (left panel) and global Zak phase in trivial/nontrivial topological phases (right panel). Both the energy bands and the corresponding eigenfunctions come back to their initial values after two circles. Parameters are (a), (b) $\theta=-0.6\pi$, (c), (d) $\theta=0.3\pi$, (e), (f) $\theta=-0.1\pi$, and (g), (h) $\theta=-0.9\pi$ with $g_1=\gamma=1$, $\delta=\sqrt{3}+(1/2)\sin\theta$, $g_2=1+(1/2)\cos\theta$. In (b), (d), (f), and (h), solid black lines indicate numerical results of global Zak phase in Eq. (13); red dashed lines indicate numerical results in the Wilson loop approach in Eq. (11).

## 5. Conclusion

We have investigated the topological properties of a $\mathcal{PT}$-symmetric non-Hermitian rhombic lattice. The bulk–boundary correspondence of the lattice is valid and the topological properties are encoded in the bulk Bloch Hamiltonian. The topological edge states present in the two band gaps in the topologically nontrivial phase. In addition, the anomalous edge states localized in two diamond plaquettes are induced by the destructive interference when all energy bands are flat. The Wilson loop approach is employed to acquire the global Zak phase for the topological characterization of the trimerized model. The global Zak phase is nonzero in the nontrivial phase, and the global Zak phase vanishes in the trivial phase. Our findings uncover the topological properties of the $\mathcal{PT}$-symmetric non-Hermitian rhombic lattice and provide a prototypical approach for obtaining the topological properties of the 1D multi-band non-Hermitian topological phases.

## Acknowledgment

Project supported by the National Natural Science Foundation of China (Grants Nos. 11975128 and 11874225).

## References


[1] Feng L, El-Ganainy R and Ge L 2017 *Nat. Photon.* **11** 752
[2] Gupta S K, Zou Y, Zhu X Y, Lu M H, Zhang L J, Liu X P and Chen Y F 2019 *Adv. Mater.* **32** 1903639
[3] Zhang S Y, Fang M F, Zhang Y L, Guo Y N, Zhao Y J and Tang W W 2015 *Chin. Phys. B* **24** 090304
[4] Zhao L C, Yang Z Y and Yang W L 2019 *Chin. Phys. B* **28** 010501
[5] Dong Y, Zhang W J, Liu J and Xie X T 2019 *Chin. Phys. B* **28** 114202
[6] Zhao W L, Gong P, Wang J and Wang Q 2020 *Chin. Phys. B* **29** 120302
[7] Zhang D, Li X S, Zhang L L, Fan D Z, Jin Z and Gong W J 2020 *J. Opt. Soc. Am. B* **37** 3407
[8] Wen J, Zheng C, Kong X, Wei S, Xin T and Long G 2019 *Phys. Rev. A* **99** 062122
[9] Mao X, Qin G Q, Yang H, Zhang H, Wang M and Long G L 2020 *New J. Phys.* **22** 093009
[10] Bian Z, Xiao L, Wang K, Zhan X, Onanga F A, Ruzicka F, Yi W, Joglekar Y N and Xue P 2020 *Phys. Rev. Research* **2** 022039
[11] Zheng C, Hao L and Long G L 2013 *Phil. Trans. R. Soc. A.* **371** 20120053
[12] Jin L and Song Z 2009 *Phys. Rev. A* **80** 052107
[13] Wang Y Y and Fang M F 2018 *Chin. Phys. B* **27** 114207
[14] Hao X Z, Zhang X Y, Zhou Y H, Li W, Hou S C and Yi X X 2021 *Phys. Rev. A* **103** 053508
[15] Xiao L, Deng T, Wang K, Wang Z, Yi W and Xue P 2021 *Phys. Rev. Lett.* **126** 230402
[16] Jiang Z S, Hu D J, Pang L, Gao F H and Wang P 2018 *Chin. Phys. B* **27** 054201
[17] Cao P C and Zhu X F 2021 *Chin. Phys. B* **30** 030505
[18] Wang H, Qin Y, Ma J, Shen H, Hu Y and Jia X 2021 *Chin. Phys. B* **30** 050301
[19] Zhang S M, Zhang X Z, Jin L and Song Z 2020 *Phys. Rev. A* **101** 033820
[20] Jin L, Wu H C, Wei B B and Song Z 2020 *Phys. Rev. B* **101** 045130
[21] Jin L 2018 *Phys. Rev. A* **97** 012121
[22] Zheng C, Tian J, Li D, Wen J, Wei S and Li Y 2020 *Entropy* **22** 812
[23] Chen C, Jin L and Liu R B 2019 *New J. Phys.* **21** 083002
[24] Jiang H, Lang L J, Yang C, Zhu S L and Chen S 2019 *Phys. Rev. B* **100** 054301
[25] Ge Z Y, Zhang Y R, Liu T, Li S W, Fan H and Nori F 2019 *Phys. Rev. B* **100** 054105
[26] Wang X Y, Chen H Z, Li Y, Li B and Ma R M 2016 *Chin. Phys. B* **25** 124211
[27] Liu J S, Han Y Z and Liu C S 2019 *Chin. Phys. B* **28** 100304
[28] Liu H, Su Z, Zhang Z Q and Jiang H 2020 *Chin. Phys. B* **29** 050502
[29] Jiang X P, Qiao Y and Cao J 2021 *Chin. Phys. B* **30** 077101
[30] Liu H, Zhou J K, Wu B L, Zhang Z Q and Jiang H 2021 *Phys. Rev. B* **103** 224203
[31] Teo W X, Li L, Zhang X and Gong J 2020 *Phys. Rev. B* **101** 205309
[32] Xiao Y X, Ding K, Zhang R Y, Hang Z H and Chan C T 2020 *Phys. Rev. B* **102** 245144
[33] Liu T, He J J, Yoshida T, Xiang Z L and Nori F 2020 *Phys. Rev. B* **102** 235151
[34] Zhang X, Li G, Liu Y, Tai T, Thomale R and Lee C H 2021 *Commun. Phys.* **4** 47
[35] Wang X R, Guo C X and Kou S P 2020 *Phys. Rev. B* **101** 121116
[36] Luo X W and Zhang C 2019 *Phys. Rev. Lett.* **123** 073601
[37] Zhao X M, Guo C X, Kou S P, Zhuang L and Liu W M 2021 *Phys. Rev. B* **104** 205131
[38] Tang L Z, Zhang L F, Zhang G Q and Zhang D W 2020 *Phys. Rev. A* **101** 063612
[39] Zhai L J, Huang G Y and Yin S 2021 *Phys. Rev. B* **104** 014202
[40] Chen R, Chen C Z, Zhou B and Xu D H 2019 *Phys. Rev. B* **99** 155431
[41] Zhou L 2020 *Phys. Rev. B* **101** 014306
[42] Wu H and An J H 2020 *Phys. Rev. B* **102** 041119
[43] Bao X X, Guo G F, Du X P, Gu H Q and Tan L 2021 *J. Phys.: Condens. Matter* **33** 185401
[44] Wu Y J, Liu C C and Hou J 2020 *Phys. Rev. A* **101** 043833
[45] Yang X, Cao Y and Zhai Y 2022 *Chin. Phys. B* **31** 010308
[46] Zeng Q B, Yang Y B and Lü R 2020 *Phys. Rev. B* **101** 125418
[47] Guo C X, Wang X R and Kou S P 2020 *Phys. Rev. B* **101** 144439
[48] Murakami S, Nagaosa N and Zhang S C 2004 *Phys. Rev. Lett.* **93** 156804
[49] Wang Z, Sun Y, Chen X Q, Franchini C, Xu G, Weng H, Dai X and Fang Z 2012 *Phys. Rev. B* **85** 195320
[50] Liu Z, Kovrizhin D L and Bergholtz E J 2013 *Phys. Rev. B* **88** 081106
[51] Liu Z K, Zhou B, Zhang Y, Wang Z J, Weng H M, Prabhakaran D, Mo S K, Shen Z X, Fang Z, Dai X, Hussain Z and Chen Y L 2014 *Science* **343** 864
[52] Xiao M, Ma G, Yang Z, Sheng P, Zhang Z Q and Chan C T 2015 *Nat. Phys.* **11** 240
[53] Weng H, Fang C, Fang Z, Bernevig B A and Dai X 2015 *Phys. Rev. X* **5** 011029
[54] Lu L, Wang Z, Ye D, Ran L, Fu L, Joannopoulos J D and Soljačić M 2015 *Science* **349** 622
[55] Yi Y and Yang Z 2020 *Phys. Rev. Lett.* **125** 186802
[56] Qin C, Wang B, Wong Z J, Longhi S and Lu P 2020 *Phys. Rev. B* **101** 064303
[57] Qin S, Hu L, Le C, Zeng J, Zhang F C, Fang C and Hu J 2019 *Phys. Rev. Lett.* **123** 027003
[58] Yang Z, Zhang K, Fang C and Hu J 2020 *Phys. Rev. Lett.* **125** 226402
[59] Yang Z, Chiu C K, Fang C and Hu J 2020 *Phys. Rev. Lett.* **124** 186402
[60] Xu Z and Chen S 2020 *Phys. Rev. B* **102** 035153
[61] Liu C H, Zhang K, Yang Z and Chen S 2020 *Phys. Rev. Research* **2** 043167
[62] Zhu B, Lü R and Chen S 2014 *Phys. Rev. A* **89** 062102
[63] Bai W K, Yang T and Liu W M 2020 *Phys. Rev. A* **102** 063318
[64] Wang H Y, Zheng Z, Zhuang L, Tai Y H, Shi J S and Liu W M 2020 *J. Phys.: Condens. Matter* **32** 235701
[65] Wu Y J, Gao T B, Li N, Zhou J and Kou S P 2020 *J. Phys.: Condens. Matter* **32** 145601
[66] He J, Kong X, Wang W and Kou S P 2018 *New J. Phys.* **20** 053019
[67] Yao S and Wang Z 2018 *Phys. Rev. Lett.* **121** 086803
[68] Wang H, Ruan J and Zhang H 2019 *Phys. Rev. B* **99** 075130
[69] Yang Z and Hu J 2019 *Phys. Rev. B* **99** 081102
[70] Su W P, Schrieffer J R and Heeger A J 1979 *Phys. Rev. Lett.* **42** 1698
[71] Liu J S, Han Y Z and Liu C S 2020 *Chin. Phys. B* **29** 010302
[72] Zhao X, Xing Y, Qi L, Liu S, Zhang S and Wang H F 2021 *New J. Phys.* **23** 073043
[73] Lang L J, Weng Y, Zhang Y, Cheng E and Liang Q 2021 *Phys. Rev. B* **103** 014302
[74] Li S, Liu M, Li F and Liu B 2021 *Phys. Scr.* **96** 015402

[75] Xu K, Zhang X, Luo K, Yu R, Li D and Zhang H 2021 *Phys. Rev. B* **103** 125411
[76] Lin Q, Xiao M, Yuan L and Fan S 2016 *Nat. Commun.* **7** 13731
[77] Wang L, Liu Q and Zhang Y 2021 *Chin. Phys. B* **30** 020506
[78] Zhang X X and Franz M 2020 *Phys. Rev. Lett.* **124** 046401
[79] Shen H, Zhen B and Fu L 2018 *Phys. Rev. Lett.* **120** 146402
[80] Liu F and Wakabayashi K 2021 *Phys. Rev. Research* **3** 023121
[81] Xu Y, Wang S T and Duan L M 2017 *Phys. Rev. Lett.* **118** 045701
[82] Liang S D and Huang G Y 2013 *Phys. Rev. A* **87** 012118
[83] Leykam D, Bliokh K Y, Huang C, Chong Y D and Nori F 2017 *Phys. Rev. Lett.* **118** 040401
[84] Lin S, Jin L, and Song Z 2019 *Phys. Rev. B* **99** 165148
[85] Song F, Yao S and Wang Z 2019 *Phys. Rev. Lett.* **123** 246801
[86] Zhu B, Ke Y, Zhong H and Lee C 2020 *Phys. Rev. Research* **2** 023043
[87] Wang X, Xiao L, Qiu X, Wang K, Yi W and Xue P 2018 *Phys. Rev. A* **98** 013835
[88] Lee T E 2016 *Phys. Rev. Lett.* **116** 133903
[89] Jin L and Song Z 2019 *Phys. Rev. B* **99** 081103
[90] Yao S, Song F, and Wang Z 2018 *Phys. Rev. Lett.* **121** 136802
[91] Zhang K, Yang Z and Fang C 2020 *Phys. Rev. Lett.* **125** 126402
[92] Jin L 2017 *Phys. Rev. A* **96** 032103
[93] Wu H C, Jin L, and Song Z 2021 *Phys. Rev. B* **103** 235110
[94] Qin W, Li, L and Zhang Z 2019 *Nat. Phys.* **15** 796
[95] Skagerstam B S 1992 arXiv:hep-th/9210054
[96] Wang H X, Guo G Y and Jiang J H 2019 *New J. Phys.* **21** 093029